Journal of Applied Fluid Mechanics, Vol. 11, No. 5, pp. 1231-1237, 2018.
Available online at www.jafmonline.net, ISSN 1735-3572, EISSN 1735-3645.
DOI: 10.29252/jafm.11.05.28507

CFD-Based Optimization of Micro Vortex Diodes

K. Fouladi† and J. Czupryna

Department of Mechanical Engineering, Widener University, University Place, Chester, PA 19013, USA

†*Corresponding Author Email: kfouladi@widener.edu*

(Received October 9, 2017; accepted May 45, 2018)

ABSTRACT

Microvalves can play an essential role in transport and control of fluids for biomedical applications. These valves may face reliability issues as they can fail due to deterioration of the moving parts exposed to prolonged and repeated movements or handling fluids that contain particles of several microns in diameter. An alternative to valves with moving parts are microdiodes such as micro vortex diode, which offers high resistance to flow in one direction and much smaller resistance in the opposite direction. The present study is focused on developing a two-step computationally-based approach for design and optimization of micro vortex diodes. A numerical design optimization based on the Design of Experiment and Response Surface Method is employed to improve the efficiency of a micro vortex diode using geometrical parameters. The results of the optimization study suggest an optimal design with about 69% improvement in efficiency compared to the reference design.

Keywords: Micro vortex diode; Miodicity; Pressure drop; Simulation; CFD; Optimization; Design of experiment; Response surface method.

NOMENCLATURE

a	diode diameter
a_i	design variable factors
D	hydraulic diameter
d	diode depth
Di	diodicity
f	surface representation
il	lower bound
iu	upper bound
k	number of design variables
n_c	number of constraints
P	pressure
Q	flow rate
Q_f	flow rate in forward direction
Q_r	flow rate in reverse direction
Re	Reynolds number
U	velocity component
$\boldsymbol{V}$	velocity vector
w	tangential port height
x	design variables
y	objective function
ΔP	pressure difference
ε	noise or error
μ	viscosity
ρ	density
η	efficiency
T	viscous stress

1. INTRODUCTION

Microfluidic devices have shown great potential for biomedical applications. These devices may be used in drug delivery, biological detection, cellular analyses, tissue engineering, etc. (Li and Zhou 2013). Among fluidic microsystems, microvalves can play an essential role in fluid transport and control phenomena (Au *et al.* 2011). Microvalves allow the user to control the fluid macroscopic parameters. A major class of microvalves are valves that can be actuated mechanically (Anduze *et al.* 2001). Microvalves with moving mechanical parts (MVMPs) can pose major manufacturing difficulties. Additionally, these valves may have reliability issues as they can fail due to deterioration of the moving parts exposed to prolonged and repeated movements. For example, many biological and medical applications require handling fluids that contain particles of several microns in diameter. These particles can render microvalves dysfunctional by either damaging the valve seats if they are hard or adhering to the seat if they are soft (Anduze *et al.* 2001).

The repair or replacement of MVMPs can be

either cost prohibitive or unsafe for some applications. An alternative to MVMPs are microdiodes, which offer high resistance to flow in one direction and much smaller resistance in the opposite direction (Zobel 1936; Kulkarni *et al*. 2008; Escudier 1982; Olsson 1995; Forster 1995; Gerlack 1998). An example of such a device is the vortex diode. The vortex diode is designed with a disc-shaped chamber with an axial port and a tangential port. It allows the flow in the forward direction enter at the center of the device and exit at the tangential port with relatively small pressure drop. In the reverse direction, the flow enters the tangential port creating a rotating and swirling flow in the diode chamber and then exits at the axial port. The swirling flow results in significantly larger pressure drop in the reverse direction compared to the forward direction (Yoder 2012). An example of the forward and the reverse flow directions in the vortex diode is shown in Fig. 1. In this example, with the flow rate set at $Q = 5.54\,x10^{-8}\frac{m^3}{s}$ $(Re = 275)$, the computed pressure drop in the diode for the forward direction is $43\,kPa$ compared to $81\,kPa$ for the reverse direction.

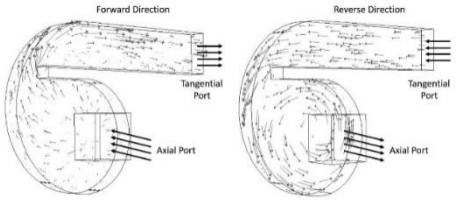

Fig. 1. Vortex diode flow directions

Vortex diodes have been used as leaky non-return valves in a variety of applications. For example, they are utilized in the nuclear industry as radioactive waste pumping system with no moving parts (Yoder, 2012). In hydraulic/thermal power stations, they are mainly used to dampen the oscillations in pipe systems (Haakh 2003). They have also been proposed as part of a ship's ballast water filtration and disinfection system (Kulkarni *et al.* 2008). For these applications, the vortex diodes are generally designed and manufactured at macroscale (millimeters to meters).

A significant amount of research has been conducted for both design and optimization of vortex diodes. However, the majority of these works have been performed for macroscale sized diodes. These studies have resulted in a good understanding of flow behavior at the macroscale (Kulkarni *et al.* 2008; Yoder 2012; Haakh 2003; Bardell 2000; Pandare and Renade 2015). For example, it has been stated that the efficiency of the macro vortex diode depends largely on the competition between the inertial and viscous effects (Anduze *et al.* 2001). In these diodes, the extent of laminar or turbulent nature of the flow has a significant influence on the pressure drop. More specifically, Reynolds number has a strong influence on the efficiency of the macro vortex diode.

The results obtained in the macroscale may not be useful for vortex diodes designed for biomedical applications, which are often sized in microscale. For example, microscale vortex diodes have shown to performance poorly compared to macroscale diodes (Bardell 2000). This is due to the fact that smaller dimensions of the micro vortex diodes would result in flow remaining laminar and not allowing for direct exploitation of significant inertial losses similar to the macro vortex diodes (Anduze *et al.* 2001). Therefore, some basic research focused on micro vortex diodes is needed to identify the geometrical and flow variables that can have significant effects on the efficiency of these diodes and then use those parameters for performance optimization of these configurations.

The present effort is focused on developing a computationally based methodology for design and optimization of a micro vortex diode. In this effort, the effects of various geometrical parameters such as diode diameter, diode depth, and tangential port height on the performance of the diode are investigated. Subsequently, a numerical design optimization based on the Design of Experiment and Response Surface Method is employed to improve the efficiency of the micro vortex diode using only the geometrical parameters that have shown to have significant effects on the diode performance.

2. NUMERICAL ANALYSIS

The present effort utilizes a two-step approach for design and optimization of a micro diode configuration using computational fluid dynamics modeling. In Step 1, the effects of several geometrical parameters on the micro vortex diode performance are investigated. These parameters include diode diameter, diode depth, and tangential port height. This portion of the study investigates if any of these geometrical parameters show a significant effect on the diode performance. Geometrical parameters that affect diode performance are then considered as design variables considered in the next step, which is focused on the performance optimization of the micro vortex diode.

2.1 Simulation setup and validation

The reference micro vortex diode investigated in the present study is shown in Fig. 2. This configuration was originally developed by Anduze *et al.* (2001) and is made of a rectangular duct, which is tangentially connected to a spiral central chamber and the orifice is positioned in the center of the spiral chamber. Both forward and reverse directions of the flow in this diode are illustrated in Fig. 1.

For the reverse direction, a vortex occurs in the chamber as the flow enters the tangential port (See Fig. 1) causing significant pressure drop due to the viscous dissipation in the eddy. Conversely, in the forward direction, the fluid enters the chamber through the axial orifice and it

exits from the tangential duct without significant circulation and with less pressure drop. Shown in Fig. 3, the streamlines patterns colored with static pressure values inside diode illustrate the described flow behaviors.

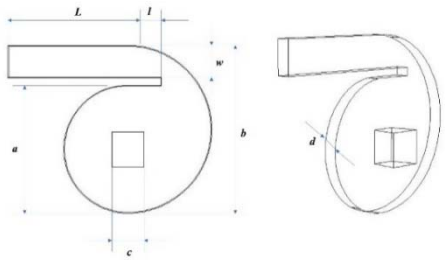

Fig. 2. Schematic representation of reference vortex diode from Anduze *et al.* [3]

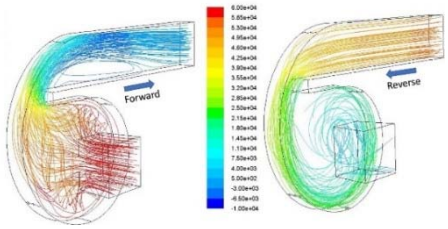

Fig. 3. Streamlines patterns colored with static pressure values for both forward and reverse directions

The reference diode configuration used for validation of the numerical model is created using the following specifications: $a = 500\,\mu m$, $b = 750\,\mu m$, $c = 150\,\mu m$, $d = 80\,\mu m$, $l = 210\,\mu m$, $L = 750\,\mu m$, and $w = 200\,\mu m$ (Fig. 2). A grid dependency study was carried out to find an optimum mesh of about 280,000 total elements with ten inflation layers near wall boundary. The mesh independent study was performed on the reference diode configuration at the nominal flow rate of $Q = 5.54\,x10^{-8}\frac{m^3}{s}$ using diodicity (defined in Section 2.3) as the figure of merit. A representative of the tetrahedral grid system employed for the CFD simulation is shown in Fig. 4.

Fig. 4. Fully unstructured tetrahedra surface mesh representative.

The numerical modeling for the flow analyses and optimization of the micro vortex diode is performed using the finite volume-based commercial software ANSYS Fluid® as the pressure-based flow solver (ANSYS 2017). SIMPLE scheme with second-order spatial discretization for pressure and second-order upwind scheme for momentum equation is used in the numerical simulations. Water is used as the working fluid with constant properties at $T = 298\,K$ and all simulations are performed assuming laminar flow regime. The assumption of laminar flow will be explained in detail later. Therefore, the following continuity and momentum equations are solved for transient, three-dimensional, incompressible flow fields:

$$\nabla \cdot \boldsymbol{V} = 0 \tag{1}$$

$$\rho\left(\frac{\partial \boldsymbol{V}}{\partial t} + \boldsymbol{V} \cdot \nabla \boldsymbol{V}\right) = -\nabla P + \nabla \mathbf{T} \tag{2}$$

where ρ is density, $\boldsymbol{V}$ is velocity, P is pressure, and $\mathbf{T}$ is viscous stress.

The numerical setup and meshing used in the analyses are validated against the experimental data that were presented in [3]. The experiment by Anduze *et al*. [3] was conducted with water at $T = 298$ K, which is also used in the present effort. Anduze *et al*. defined Reynolds numbers as,

$$Re = \frac{\rho\, U\, D}{\mu} \tag{3}$$

where U and D are the velocity and hydraulic diameter at the smallest cross-section of the flow, respectively. Parameters ρ and μ are density and dynamic viscosity of the fluid, respectively. They indicated that the Reynolds number at the smallest cross-section for all cases were calculated between 100 and 800 indicating the flow to remain laminar in the diode for all cases (Anduze *et al.* 2001). CFD results also indicate similar range for Reynolds number, which verifies the laminar assumption in the numerical analyses.

The comparison of the pressure difference (ΔP) and volumetric flow rate (forward Q_f and reverse Q_r) between computational results of the present study and experimental data from Anduze *et al.* 2001 is shown in Fig. 5. In the experiment of Anduze *et al.* 2001, these parameters were directly measured. In the numerical simulation, they are obtained from the integration of the local static pressures and velocities calculated at the inlet and the outlet of the diode configuration. Overall, Fig. 5 shows good agreement between experimental data and numerical simulation with the highest discrepancy at about 7%. It should be noted that for these cases, the pressure difference between inlet and outlet of the diode are set as boundary conditions and volume flow rate through the diode is obtained from the simulations.

In their study, Pandare and Ranade (2015) discussed the convergence difficulties for the continuity equation if the steady solver is used for simulation of flows in vortex diodes. They argued that these difficulties arise due to the precession

of the vortex core and recommended using a transient solver to achieve convergence. Their recommendation was implemented herein. For these cases, in addition to the residuals, the area-weighted average values of pressure at the inlet and velocity at the outlet of the diode chamber are monitored to ensure convergence. Furthermore, time-step used in the simulations is adjusted with flow rate.

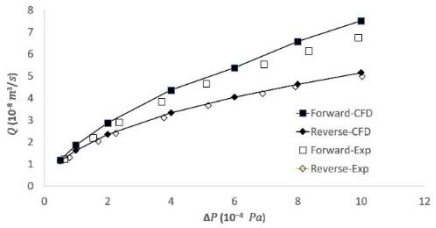

Fig. 5. Comparison of numerical and experimental flow rates with liquid water at $T = 293\ K$

2.2 Boundary Conditions

The present study included three different sets of simulation. The first simulation set was focused on validation of the model. For all runs in this set, the pressure difference between inlet and outlet of the diode were set as boundary conditions, and volume flow rate through the diode is obtained from the simulations. For forward direction, the pressure inlet boundary condition was used at the axial port and pressure outlet at the tangential port. For the reverse flow, inlet pressure was used at the tangential port and outlet pressure at the axial port. The boundary conditions and ports are shown in Fig. 6.

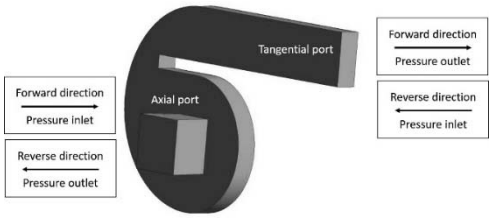

Fig. 6. Boundary conditions for validation cases.

For Geometrical effects runs in the second set, the mass flow rate of $\dot{m} = 5.47\ x10^{-5}\ \frac{kg}{s}$ is set as the inlet boundary condition (axial port in forward direction and tangential port in reverse direction) and ambient pressure $(101325\ Pa)$ is set at the outlet condition (Fig. 7) . These boundary conditions allowed to obtain the inlet pressure from the simulations.

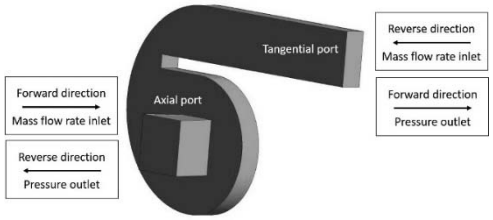

Fig. 7. Boundary conditions for geometrical effects cases.

The boundary condition for optimization runs in the third set were specified similar to validation cases (Fig. 6). However, in this set, the pressure drop of ΔP=80,000 pa was specified as boundary conditions for all forward and reverse direction cases allowing to compute diode volume flow rates from the simulations.

2.3 Performance metrics

Past studies have used two different metrics to measure the effectiveness of vortex diodes. The first and most prevalent metric is diodicity (Di), defined as

$$Di = \frac{\Delta P_r}{\Delta P_f} \tag{4}$$

where ΔP_r is the reverse pressure drop and ΔP_f is to the forward pressure drop, both at the same flow rate (Fadl *et al.* 2010). The second metric to measure the effectiveness of vortex diodes is efficiency. For a given pressure drop in both forward and reverse flow directions, the diode efficiency is defined as

$$\eta = \frac{Q_f - Q_r}{Q_f} \tag{5}$$

where Q_f is the volume flow rate in the forward direction and Q_r is the volume flow rate in the reverse direction (Anduze *et al.* 2001). Both Di and η are used in the present study to establish and improve the performance of the micro vortex diode.

2.4 Optimization Process

A design optimization process is generally focused on minimizing or maximizing an objective function, $y(x)$, subjected to constraint functions (Katoozian 1993)

$$y_j(x) \leq 0\ ;(j = 1,2,3,\dots n_c) \tag{6}$$

within the design space

$$x_{il} \leq x_i \leq x_{iu} \tag{7}$$

where $x = [x_1, x_2, \dots x_k]$ is the design variable vector with x_{il} and x_{iu} as the physical upper and lower bounds, respectively. Parameters n_c and k represent the number of constraints and the number of design variables, respectively.

The application of Response Surface Method (RSM) to design optimization is aimed at reducing the cost of computationally expensive simulations such as finite element method or CFD and numerical noise associated with these analyses. RSM can be used to streamline the design optimization process and reduce design's computational cost and time (Yi *et al.* 2012). Background and some details on the RSM can be found in Guo and Zhang (2004), Ren and Chen (2010), and Cho *et al.* (2011). A response surface can be defined as

$$y = f(x_1, x_2) + \varepsilon \tag{8}$$

where ε represents the noise or error observed in the response y and the surface represented by

$f(x_1, x_2)$. A response surface mathematical model approximates the objective functions of the system in design space. A second-order polynomial function with interaction effect is typically adequate for representing physical systems for many engineering applications such as the present study:

$$y = a_0 + a_{i....n}x_{i....n} + \sum_{i=1}^{N} a_i x_i + \sum_{i\neq j}^{N} a_i x_i x_j + \sum_{i\neq j\neq k}^{N} a_i x_i x_j x_k \quad (9)$$

where y presents the objective output, x_i is the design variable, and coefficients a_i are the effects of the x_i factors. In the present method ANSYS Design Xplorer® (ANSYS 2017) is employed to create response surface of the single design variable using the second-order polynomial response surface method. Moreover, the Min-Max principle with the screening algorithm is used as the search engine to find the maximum of the design variable, diode efficiency η.

3. Results & Discussion

3.1 Step 1 – Geometrical effects

Figure 8 shows the effects of diode diameters (a), diode depth (d), and tangential port height (w) on the diodicity of the micro vortex diode. The geometrical parameters shown in Fig. 8 are non-dimensionalized using their respective reference geometry values (i.e., $a_{ref} = 500\ \mu m$, $d_{ref} = 80\ \mu m$, and $w_{ref} = 200\ \mu m$) (Anduze *et al.* 2001).

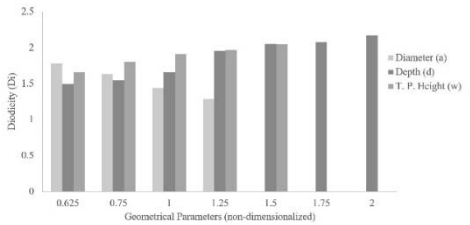

Fig. 8. Effects of geometrical parameters (diode depth, diode diameter, and tangential port height) variation on diode diodicity.

For these runs, volume flow rate of $Q = 5.54\ x10^{-8}\frac{m^3}{s}$ is set as the inlet boundary condition and ambient pressure ($101325\ Pa$) is set at the outlet condition allowing to obtain the inlet pressure from the simulations. All three parameters are shown to have significant effects on diodicity. The increase in diode depth increases the diode diodicity. The additional depth space may allow more room in the chamber for the flow to swirl around resulting in additional pressure losses in the reverse direction. The diodicity is also increased with increase in tangential port height. The increase in height means larger area for the tangential port. With constant volume flow rate, the increase in the area results in lower velocity or higher pressure at the tangential port. The higher tangential port pressures are observed in both forward and reverse directions with pressure values in the reverse direction greater compared to the forward direction. Conversely, larger diode diameters result in smaller diodicity as larger diameters result in lower pressure losses in the reverse direction, which may be due to lower viscous losses.

3.2 Step 2 – Performance Optimization

For CFD runs used for the optimization, the pressure difference between inlet and outlet of the diode are set as boundary conditions ($\Delta P = 80{,}000\ pa$) and the forward and reverse directions volume flow rates through the diode are obtained from the simulations. The efficiency is then calculated from these flow rates as presented in Eq. (5). The response surfaces of the objective function, diode efficiency (η), are presented in Fig. 9.

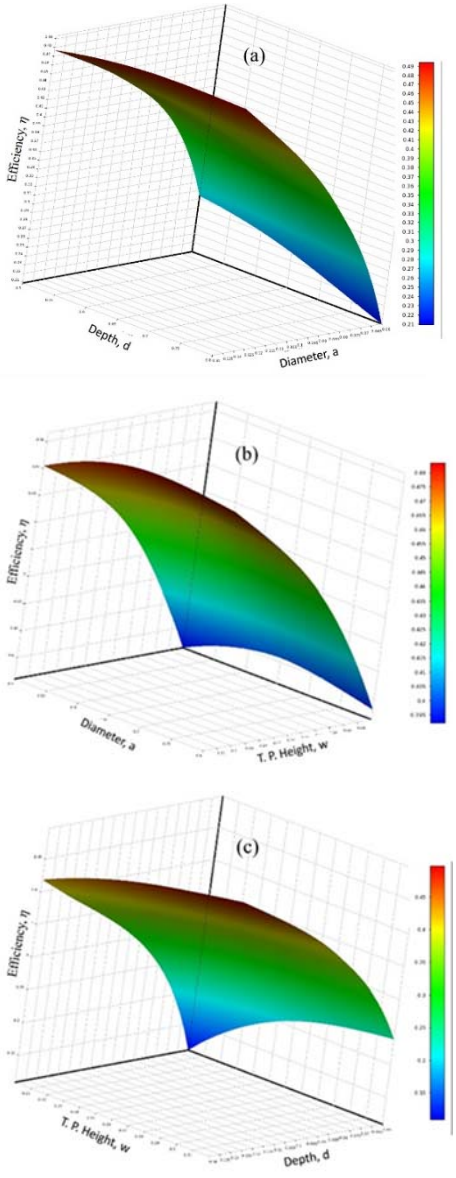

Fig. 9. Response surfaces of diode efficiency (η).

The response surfaces are generated using the CFD simulation results where the run matrix to generate the results are based on Design of Experiment through optimal space-filling design method. In Fig. 9 (a-c), the response surfaces

illustrate the variation of the objective function (efficiency) with the design variables (diode depth, diode diameter, and tangential port height) and quantify the impact of these variables on the diode efficiency.

The goodness of fit chart is presented in Fig. 10, which shows the excellent quality of the response surfaces.

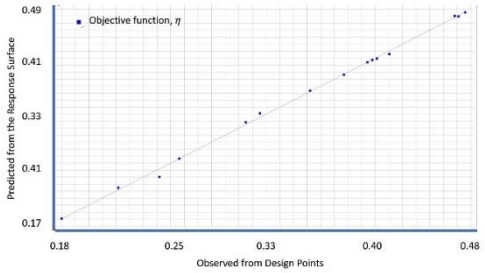

Fig. 10. Goodness of fit chart for assessing response surface quality.

Finally, Table 1 presents the comparison of the reference design and the optimal design. The results presented in this table show about 69% improvement in efficiency for the optimal design compared to the reference design. The optimization process indicates that the optimal design is attained at $a = 720\,\mu m$, $d = 140\,\mu m$, and $w = 320\,\mu m$. Furthermore, the optimal performance is achieved at higher flow rate compared to the reference design due to larger diode dimensions.

Table 1 Performance Comparison of Reference and Optimal Designs

Design	Reference	Optimal
Diameter (a), μm	500	720
Depth (d), μm	80	140
T.P. height (w), μm	200	320
Q_f , m^3/s	6.58E-08	2.02E-07
Q_r , m^3/s	4.64E-08	1.02E-07
Efficiency (η)	0.295	0.495

4. CONCLUSIONS

A two-step computational approach for design and optimization of a micro vortex diode has been presented in this study. In Step 1, the effects of several geometrical parameters on the micro vortex diode performance were investigated. The efforts in step 2 were focused on the performance optimization of the micro vortex diode through variation of the geometrical parameters considered in the previous step. These parameters included diode diameters, diode depth, and tangential port height.

The geometrical effects study showed that all three parameters to have significant effects on the diodicity. The increase in both diode depth and tangential port height resulted in higher diode diodicity, while larger diode diameters resulted in smaller diodicity. All three geometrical parameters were subsequently used in the optimization study. In the optimization step, response surfaces were generated using CFD simulation to search for an optimal design to achieve optimum diode efficiency. The results of the optimization study suggest an optimal design with about 69% improvement in efficiency compared to the reference design.

Future plans for this work involve consideration of elastic micro vortex diode configurations, which may require simulations that include strongly coupled fluid-structure interaction (FSI). Hence, new experimental work using elastic diode configurations would also be needed to validate the future FSI model.

ACKNOWLEDGEMENTS

This work used the Extreme Science and Engineering Discovery Environment (XSEDE), which is supported by National Science Foundation grant number OCI-1053575. Specifically, it used the Bridges system, which is supported by NSF award number ACI-1445606, at the Pittsburgh Supercomputing Center (PSC). Additionally, the authors sincerely appreciate the support and help provided by ANSYS, Inc.

REFERENCES

Anduze, M., S. Collin, R. Caen, H. Camen, V. Condera, and T. Do Conto (2001). Analysis and testing of a fluidic vortex microdiode. *Journal of Micromechanics and Microengineering*, 11(2), 108-112.

ANSYS, "Fluids - CFD Simulation Software | ANSYS," [Online]. Available: http://www.ansys.com/products/fluids. [Accessed 10 September 2017]

ANSYS, "Design Xplorer," ANSYS, Inc., [Online]. Available: http://www.ansys.com/products/platform/ansys-designxplorer. [Accessed 21 September 2017].

Au, A. K., H. Lai, B. R. Utela, and A. Folch (2011). Microvalves and micropumps for BioMEMS. *Micromachines*, 2(2), 179-220.

Bardell, R. L. (2000). *The diodicity mechanism of tesla-type no-moving-parts valves*. Ph.D. Dissertation, University of Washington, Seattle, Washington, USA.

Cho, C. S., E. H. Choi, J. R. Cho, and O. K. Lim (2011). Topology and parameter optimization of a foaming jig reinforcement structure by the response surface method. *Computer-Aided Design*, 43(12), 1707-1716.

Escudier, M., J. Bornstein and T. Maxworthy (1982). The dynamics of confined vortices. In *Royal Society of London A: Mathematical, Physical and Engineering Sciences.*

Fadl, A., S. Demming, A. Zhang, and S. Büttgenbach (2010). A multifunction and bidirectional valve-less rectification

micropump based on bifurcation geometry. *Microfluidics and Nanofluidics,* 9(2-3), 267-280.

Forster, F. K., R. L. Bardell, and M. A. Afromowitz (1995). Design, fabrication and testing of fixed-valve micro-pumps. In *Proceedings of the ASME Fluid Engineering Division*.

Gerlach, T. (1998). Microdiffusers as dynamic passive valves for micropump applications. *Sensors and Actuators A: Physical,* 69(2), 9-191.

Guo, Q. T. and L. M. Zhang (2004). Finite element model updating based on response surface methodology. *In 22nd international modal analysis conference*, Dearborn, MI.

Haakh, D. I. F. (2003). Vortex chamber diodes as throttle devices in pipe systems. Computation of transient flow. *Journal of Hydraulic Research,* 4(1) 53-59.

Katoozian, H. (1993). *Three dimensional design optimization of femoral components of total hip endoprostheses*. Ph.D. Dissertation, Case Western Reserve University, Cleveland, OH, 1993.

Kulkarni, A. A., V. V. Ranade, R. Rajeev, and S. B. Kogaanti (2008). CFD simulation of flow in vortex diodes. *AIChE journal,* 54(5), 1139-1152.

Li, X. J. and Z. Yu, Eds. (2013). Microfluidic devices for biomedical applications, Elsevier, Atlanta, Goergia, USA.

Olsson, A., G. Stemme, and E. Stemme (1995). A numerical design study of the valveless diffuser pump using a lumped-mass model. *Journal of Micromechanics and Microengineering,* 9(1), 34-44.

Pandare, A. and V. V. Ranade (2015). Flow in vortex diodes. *Chemical Engineering Research and Design,* 102, 274-285.

Ren, W. X. and H. Chen (2010). Finite element model updating in structural dynamics by using the response surface method. *Engineering structures,* 32(8) 2455-2465.

Yi, P. X., L. J. Dong, and Y. X. Chen (2012). The multi-objective optimization of the planet carrier in wind turbine gearbox. *Applied Mechanics and Materials,* 184 565-569.

Yoder, G. L., Y. M. Elkassabgi, and G. I. De Leon (2012). Vortex diode analysis and testing for fluoride salt-cooled high-temperature reactors (No. ORNL/TM-2011/425). Oak Ridge National Laboratory (ORNL).

Zobel, R. (1936). Experiments on a hydraulic reversing elbow. *Mitt Hydr Inst Munich,* 8, 1-47.